Ellipsometric light scattering for the characterization of thin layers on dispersed colloidal particles

Andreas Erbe, Klaus Tauer, and Reinhard Sigel
Max Planck Institute of Colloids and Interfaces, D-14476 Golm, Germany
(Received 11 November 2005; published 21 March 2006)

The thin interface layer on colloids in a liquid can be characterized by applying nulling ellipsometry to a scattering experiment. Close to 90° scattering angle the ellipsometric quantities $\tan(\Psi)$ and Δ of particles smaller than the wavelength behave like at the Brewster angle of reflection ellipsometry. The minimum of $\tan(\Psi)$ and the slope of Δ depend on thickness and refractive index of the layer, while the location of the minimum is sensitive to the refractive index of the particle. As an example, the swelling of a thermosensitive layer on colloidal particles has been determined from measurements at two wavelengths.

DOI: 10.1103/PhysRevE.73.031406 PACS number(s): 82.70.Dd, 07.60.Fs, 42.68.Mj

The stability of colloidal particles in a dispersion is largely governed by their interface to the surrounding medium. Either electrostatic repulsion by interface charges or steric interactions due to polymers anchored to the interface provide a stabilization against aggregation and subsequent precipitation [1]. Technological applications strongly depend on the stability of colloids, and therefore on the interfacial structure. Also, a lot of biological processes involve interactions at interfaces of cells and cell organells, the size of which is similar to colloidal particles. One example is oligosaccharides bound to membranes mediating interactions on different length scales in and between cells [2].

Despite its importance, experimental methods to characterize the interface of colloids in solution are not well established. The investigation of colloidal dispersions is usually done by scattering experiments. Since scattering data are not specifically sensitive to the particle's interface, the characterization of the interface requires lengthy and complicated modeling of the whole particle, in addition to data from a wide enough range of scattering vectors [3,4]. A common approach to overcome these difficulties is the application of contrast variation techniques, which hide the contribution of the colloidal core and emphasize the interface. These techniques are restricted to special samples and solvents with suitable contrast parameters (refractive index, scattering length density, or electron density) [5–7]. In the case of small-angle neutron scattering (SANS), contrast variation is done by a substitution of hydrogen atoms by deuterium [8]. Despite the common creed that such a substitution would have no effect on the sample properties, there are experiments which show differences for hydrogenated and deuterated solvents [9,10]. Tracer particles enriched at a colloidal interface can be detected by anomalous small-angle x-ray scattering (ASAXS) [11]. In addition to scattering methods, electron microscopy of a frozen or dried sample is often used to investigate shells of colloidal particles. Cryotransmission electron microscopy can be applied to image core-shell particles [7]. Since the elaborate sample preparation might cause artifacts especially for soft samples, the interpretation of the resulting pictures requires an experienced operator. A difference approach determines the total size of the particle from dynamic light scattering (DLS), while the size of the core is obtained from transmission electron microscopy (TEM) of a dry sample [12]. Here, polydispersity is an important issue, especially since the two applied experimental techniques involve different weighting of particles with different sizes. Another technique is single particle light scattering, which determines accurately the intensity differences of light scattered by coated and uncoated particles [13,14]. Since it yields the whole intensity distribution, the effect of poyldispersity is monitored. However, obviously it is restricted to particles with a soluble core and large scattering intensity.

For the characterization of thin layers on flat surfaces, reflection ellipsometry is a widely applied standard technique. Thickness and refractive index of such layers are derived from the change of polarization of light reflected at the surface [15]. In spectroscopic ellipsometry, a very high resolution below 1 nm has been proven experimentally [16]. Note that the layer thickness is the first moment of the refractive index profile and not a local quantity. For such an integral parameter, the detection of values below the wavelength of light λ is not excluded. A quantity of similar character is the radius of gyration of a particle, for which the accepted noise limited resolution limit is $\lambda/40$.

In this paper we describe a scattering analogy to reflection ellipsometry: the combination of a scattering experiment with polarization optics of an ellipsometer is used for interface analysis of colloidal particles dispersed in a liquid. It has been noticed for a while that the change of polarization in a scattering process, usually described in terms of the Mueller or phase matrix, has the same information content than ellipsometric data [15]. However, this comparison just referred to the state of polarization of reflected or scattered light, while the connection to the interface of the scattering particles has not been established yet. The examination of the Mueller matrix of the scattering process has been used exclusively for a characterization of the shape of nonspherical particles. Since the term scattering ellipsometry is already connected to polarization analysis of off-specular light in a reflection experiment [17] we prefer the name ellipsometric scattering to emphasize the underlying bulk scattering mechanism.

Compared to other techniques mentioned above, ellipsometric light scattering has several advantages. Scattering ex-

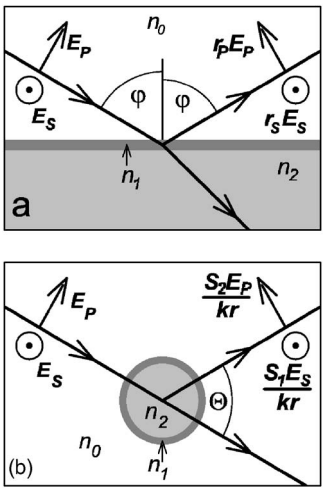

FIG. 1. Comparison of reflection ellipsometry (a) and ellipsometric scattering (b). A plane (a) or spherical (b) stratified refractive index profile n_0, n_1, n_2 leads to reflection and refraction (a) or scattering (b) of the two eigenmodes E_s and E_p of the electrical field perpendicular and parallel to the plane of reflection (a) or the scattering plane (b). Θ is the scattering angle, φ is the angle of incidence, r_s and r_p are the field reflection coefficients, S_1 and S_2 are the field scattering coefficients, and $1/(kr)$ describes the decay of an outgoing spherical wave.

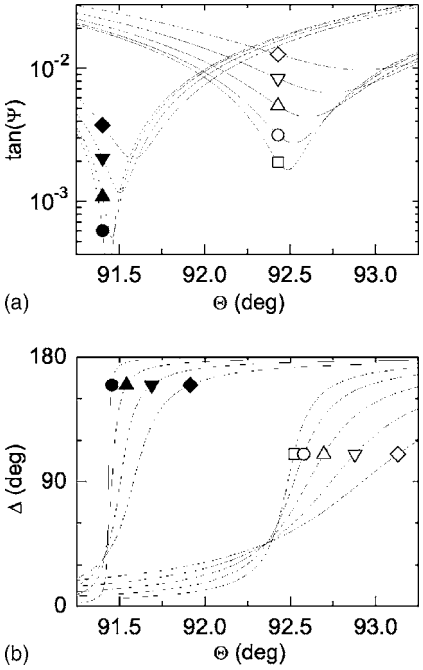

FIG. 2. Calculated scattering angle dependency of tan(Ψ) (a) and Δ (b) for a particle with a core of 100 nm radius (refractive index $n_2=1.49$) in water ($n_0=1.33$) with a shell ($n_1=1.37$) of different thickness d_s: 0 nm(□), 10 nm(●, ○), 20 nm (▲, △), 30 nm (▼, ▽), and 40 nm (◆, ◇). The curves are calculated for a light wavelength λ=633 nm (filled symbols) and λ=532 nm (open symbols).

periments in general are *in situ* methods, and effects of sample treatment can be excluded. No special solvents for contrast matching are required, as long as there is optical contrast of the interfacial structure, for instance, a particle shell, to the core and to the solvent. The core and the shell parameters are determined in a single experiment which has several benefits. It is, e.g., possible to investigate self-assembled block-copolymer micelles, where a reference sample without a corona is not available. Finally, as will be shown below, the optical contrast and therefore the swelling ratio of the corona can be determined.

The close relation between ellipsometric scattering and classical reflection ellipsometry is illustrated in Fig. 1. The latter technique is used for a characterization of thin films on plane interfaces by determining the quotient

$$\frac{r_p}{r_s} = \tan(\Psi_r)e^{i\Delta_r} \tag{1}$$

of the field reflection coefficients r_p and r_s for light with polarization parallel and perpendicular to the plane of reflection [15]. The reflection coefficients are complex numbers encoding reflection amplitudes and phase shifts caused by reflection. The resulting complex quotient is usually expressed in terms of its modulus $\tan(\Psi_r)$ representing the amplitude ratio and its argument Δ_r describing the phase difference of the two polarization modes. Ellipsometric scattering measures the quotient

$$\frac{S_2}{S_1} = \tan(\Psi)e^{i\Delta} \tag{2}$$

of the two scattering amplitudes S_2 and S_1 for polarization modes E_p and E_s parallel and perpendicular to the scattering plane by applying ellipsometric polarization optics to a scattering experiment. Again the complex quotient is expressed as amplitude ratio $\tan(\Psi)$ and phase shift Δ. The discussion here is restricted to the scattering of spherical isotropic particles in a liquid, so E_p and E_s are eigenpolarizations of the experiment with no cross term present. In analogy to the calculation of reflection coefficients by matching suitable boundary conditions at a flat interface for plane waves, the Mie theory for the calculation of S_1 and S_2 is based on suitable boundary conditions for spherical waves at a spherical interface [18,19]. The representation of the incident plane wave as a superposition of spherical waves results in the series

$$S_1 = \sum_{l=1}^{\infty} \frac{2l+1}{l(l+1)} \left[a_l \frac{P_l^{(1)}(\cos\Theta)}{\sin\Theta} + b_l \frac{dP_l^{(1)}(\cos\Theta)}{d\Theta} \right],$$

$$S_2 = \sum_{l=1}^{\infty} \frac{2l+1}{l(l+1)} \left[b_l \frac{P_l^{(1)}(\cos\Theta)}{\sin\Theta} + a_l \frac{dP_l^{(1)}(\cos\Theta)}{d\Theta} \right], \tag{3}$$

where Θ is the scattering angle and $P_l^{(1)}$ are associated Legendre polynomials. The size and the refractive index profile of the particle enter the Mie coefficients a_l and b_l. Details are described in the Appendix .

Figure 2 shows calculated curves for $\tan(\Psi)$ and Δ for a colloidal particle of 100 nm core radius and different values for the shell thickness d_s for two λ. The parameters are chosen similar to the values of the experimental example dis-

cussed below. Close to $\Theta=90°$ there is a minimum in $\tan(\Psi)$, while Δ changes steeply from a value close to zero to approximately $+180°$ or $-180°$ [20]. Since this is very similar to the behavior of $\tan(\Psi_r)$ and Δ_r in reflection ellipsometry around the Brewster angle [15], we call the angle where $\tan(\Psi)$ is at minimum also a Brewster angle. Like in classical ellipsometry, it is at the Brewster angle where the sensitivity for an interface layer is most pronounced.

It is instructive to compare the Mie scattering with the prediction of the Rayleigh-Gans theory, which is equivalent to Born's approximation for particles with low contrast or sufficiently small radius [18,19]. In this approximation, S_2 and therefore $\tan(\Psi)$ [see Eq. (2)] are exactly zero at $\Theta=90°$ and the jump in Δ becomes discontinuous. The intuitive reason for this behavior is that E_p induces secondary dipoles which oscillate within the scattering plane. Since in Born's approximation the incident wave passes the particle unperturbed, all dipole axes point to $\Theta=90°$, so there is no intensity in this direction. In contrast, Mie scattering handles wave front distortions for E_p within the particles correctly. As a consequence, there is a distribution for the directions of the secondary dipoles induced by E_p resulting in a smeared out minimum of $|S_2|$. Therefore the deviation of the Brewster angle from $\Theta=90°$ is a direct and sensitive measure for effects beyond Born's approximation. The increasing significance of such effects with smaller wavelength is visible in Fig. 2, where the Brewster angle for the two wavelengths occurs at different locations. The additional dependency on optical contrast opens the possibility to extract the particle refractive index from scattering measurements. Usually it has to be determined separately by measurements of the refractive index increment dn/dc.

The discussion so far concerned particles which are smaller than the wavelength of light. For larger particles the simple Brewster angle analogy gets lost. Information about particle coating and refractive index is no longer located in a narrow scattering angle regime. More terms in the series of Eq. (3) contribute significantly and the angular dependence becomes more structured. It is this size regime where Mie theory is applied routinely and differences to Born's approximation are visible also in the angle dependent scattering intensity $I(\Theta)$. The information content of $\tan(\Psi)$ and Δ for this case will be addressed in future investigations.

Colloidal particles formed from a poly(ethylene glycol)-*block*-poly(*N*-isopropylacryl amide)-*block*-poly(methylmethacrylate) [PEG-*b*-PNIPAM-*b*-PMMA] triblock copolymer [21] in water are well suited for an experimental test of this technique. Because of a lower critical solution temperature T_0 of PNIPAM around 32 °C, the thickness and the refractive index of the shell can be varied by changing the temperature T [10,22]. While for T lower than T_0 the PNIPAM is soluble, it collapses for T higher than T_0 onto the core formed by the insoluble PMMA blocks. The concentration $c=7.7\times10^{-3}$ wt % was chosen as low as possible in order to avoid effects of interactions and multiple light scattering. The absence of such effects was cross checked in concentration dependent measurements on colloids of similar size, refractive index, and in similar low concentrations.

A commercial light scattering goniometer (ALV, Germany) was equipped with polarization optics in the sequence polarizer-compensator-sample-compensator-analyzer. This train allows illumination and detection of light with arbitrary elliptical polarization. The compensators (Bernhard Halle, Germany) are quaterwave plates for the two available laser wavelengths 532 nm (DPSS 532-400, Coherent, USA) and 633 nm (PL-3000, Polytec, Germany). The polarizers (Bernhard Halle, Germany) have an intensity extinction ratio of 10^{-8}. Polarizers and compensators are rotated individually by stepping motor driven rotational stages (Owis, Germany). For nulling ellipsometry, the first compensator was put to 45° angle to the scattering plane and the second compensator was deactivated by keeping its optical axis parallel to the transmission direction of the analyzer. An increased accuracy was achieved by a calibration of the transmission of the polarizer, for which variations with magnitude $<3\%$ have been detected. An accurate determination of the ellipsometric quantities Δ and $\tan(\Psi)$ directly connected to the angles of the polarizers at minimum intensity (nulling positions) was achieved by a two dimensional scan of the polarizers and a subsequent fit of the theoretical trigonometric polynomial. The scan range was chosen large enough to establish two zone averaging [15], for which most imperfections of the optical elements and adjustment errors vanish in first order perturbation theory. The dominant remaining error originates from stress birefringence of the optical windows. This imperfection shows up in a constant shift of Δ, while $\tan(\Psi)$ is not affected in first order [15]. For a compensation, a shifting constant δ was added to the measured values of Δ. Measurements away from $\Theta=90°$ where $\Delta=0^{\circ}$ or $\Delta=\pm180°$ is expected yielded $\delta=(8.7\pm0.5)°$ (633 nm) and $\delta=(11.9\pm0.6)°$ (532 nm) reproducibly.

Figure 3(a) shows data and a simultaneous fit for $\tan(\Psi)$ and Δ for the two wavelengths of light at $T=32$ °C. The fit procedure used was a simulated annealing coupled to a downhill simplex method, while the standard errors were determined using the "bootstrap method" [23]. As a simple model Mie scattering of a homogeneous sphere with a homogeneous coating [18,19] is used. The core radius r_c, the shell thickness d_s and its refractive index n_s are three adjustable parameters, while the solvent and the core refractive indexes were kept fixed at the bulk values of water ($n_0=1.335$) and PMMA ($n_2=1.491$) [24], respectively.

The temperature dependence of the parameters up to 34 °C is displayed in Fig. 3(b). At higher temperatures the particles aggregate, as detected by dynamic light scattering (DLS) measurements [25] and deviations in the fits for ellipsometric light scattering data. The constant value of r_c shows that the model is appropriate. The shell thickness in contrary decreases with increasing temperature and compares well with r_h-r_c, where r_h is the hydrodynamic radius determined by DLS. The data for n_s are more noisy but support an increase with temperature, as expected for the deswelling of PNIPAM. For a calculation of the swelling ratio, the bulk refractive index of PNIPAM $n_P=1.52$ was estimated from dn/dc data [26]. As a result, the water volume content in the PNIPAM layer at $T=34$ °C before the particle aggregation is still 2/3.

A comparison of ellipsometric scattering and the contrast

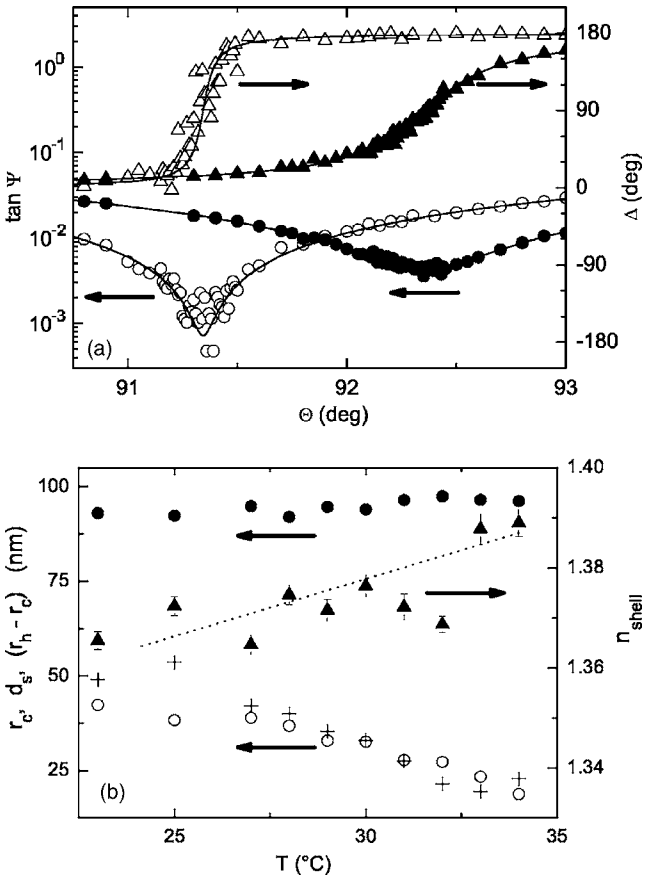

FIG. 3. (a): Data for Δ (▲, △) and tan(Ψ) (●, ○) measured at the light wavelength $\lambda=633$ nm (filled symbols) and $\lambda=532$ nm (open symbols) and the simultaneous fit (—) for the PMMA-PNIPAM-PEG colloids at the temperature $T=32$ °C. (b) Temperature dependence of the core radius r_c (●), the shell thickness d_s (○), the difference r_h-r_c of the hydrodynamic radius r_h and r_c(+), and the shell refractive index n_s (▲).

variation techniques mentioned before elucidates the special features of our method. In both cases the detected intensity is minimized, either by adjusting the polarization optics or by contrast matching of particle core and solvent. The information about the shell structure is contained in the angle dependence of either the nulling position of the polarizers directly connected to tan(Ψ) and Δ or the remaining intensity. However, ellipsometry is more than just a special case of contrast matching, since the amplitude ratio S_2/S_1 and especially the detection of the phase shift Δ is fundamentally different from the scattering intensities $|S_1|^2$ or $|S_2|^2$. A discussion of the advantages for the investigation of poyldisperse samples will be the subject of a forthcoming paper. An inherent advantage of ellipsometric scattering is its high flexibility since it requires only a simple light scattering apparatus. Applications, e.g., in process control of chemical industry are feasible. In contrast, for SANS or ASAXS, a nuclear reactor or a synchrotron is required.

In conclusion it has been shown by calculations and by experiments that ellipsometric characterization of layers on colloidal particles in solution is feasible. The position of the minimum of tan(Ψ) is an indicator for effects beyond Born's approximation and the depth of the minimum is sensitive to the thickness and the refractive index of the coating. Future investigations will concern the effects of wavelength, beam profile, multiple scattering, polydispersity, and particle interactions on ellipsometric scattering.

Since all scattering techniques share the underlying principle of interfering radiation, the results and possibilities presented here are not restricted to light scattering. In fact, spherical symmetric core shell structures occur in different branches of physics, starting from astronomy over clusters and alkali atoms to the shell model in nuclear physics. Although technically difficult or even impossible, it is clear that ellipsometric scattering experiments for these systems give similar information for the corresponding shells.

We thank Markus Antonietti for fruitful discussions. Financial support of the Max-Planck-Gesellschaft is gratefully acknowledged.

APPENDIX

The calculation of the amplitude coefficients a_l and b_l for a multilayered sphere is described in the book of Kerker [18]. Our brief summary of the relevant arguments and equations cannot substitute a complete discussion of Mie scattering. However, it provides the equations needed to obtain the results of this paper. Instead of the original solution scheme based on determinants we discuss a matrix method. This procedure is in analogy to the treatment of reflection coefficients for a planar stratified interface as described, e.g., in the excellent book of Lekner [27]. In addition to numerical advantages it yields a more clear physical picture.

For a simplified description, the scattering of electromagnetic waves at a spherical particle usually is traced back to a scalar wave problem by the introduction of Debye potentials π_1 and π_2. In spherical coordinates the resulting wave equation is separable. Here, only the radial part $R_j(r)$ $(j=1,2)$ of the Debye potentials is of interest [18]. For shells of constant refractive index the related differential equation reads

$$\frac{d^2rR_j(r)}{dr^2} + \left[k^2 - \frac{l(l+1)}{r^2}\right] rR_j(r) = 0, \tag{A1}$$

where the independent variable r is the radius, $k=2\pi n(r)/\lambda$ is the propagation constant, and l is a non-negative integer which enters through the separation from the angular degrees of freedom and indicates the angular momentum of the solution. Due to the conservation of the latter the contributions of different l do not mix, so each l can be considered separately. For a spherically stratified particle with N layers and the outer medium and the core treated as layer 0 and layer $N+1$, the refractive index profile reads $n(r)=n_i$ for $r_i > r \geqslant r_{i+1}$, where r_i is the radius of the outer boundary of layer i $(i=1,2,3,\ldots,N)$, $r_0=\infty$ and $r_{N+1}=0$. Within layer i of constant refractive index n_i and appropriate propagation constant $k_i=2\pi n_i/\lambda$, the general solutions with a preset value l are the superpositions

$$rR_1^{(l)}(r) = [a_i^{(l)}\psi_l(k_i r) + c_i^{(l)}\chi_l(k_i r)]/k_i^2,$$

$$rR_2^{(l)}(r) = [b_i^{(l)}\psi_l(k_i r) + d_i^{(l)}\chi_l(k_i r)]n_i/k_i^2 \tag{A2}$$

of Ricatti-Bessel functions $\psi_l(kr)=\sqrt{\pi kr/2}J_{l+1/2}(kr)$ and $\chi_l(kr)=-\sqrt{\pi kr/2}N_{l+1/2}$, where $J_{l+1/2}(kr)$ and $N_{l+1/2}(kr)$ are the half integer order Bessel and Neumann functions. Here, a nonmagnetic medium is assumed (magnetic permeability $\mu=1$). The conservation for the tangential electric and the magnetic field components across the layer boundaries translates to a steady behavior of $d(rR_j^{(l)})/dr$ $(j=1,2)$, $n(r)^2 rR_1^{(l)}$, and $rR_2^{(l)}$. The different behavior of rR_1 and rR_2 reflects the different character of the two potentials: R_1 is connected to the transversal magnetic wave (TM), while R_2 is assigned to the transversal electric mode (TE). These boundary conditions imply the connection

$$\begin{pmatrix} a_i^{(l)} \\ c_i^{(l)} \end{pmatrix} = \underline{M}_i^{(l)} \begin{pmatrix} a_{i-1}^{(l)} \\ c_{i-1}^{(l)} \end{pmatrix},$$

$$\begin{pmatrix} b_i^{(l)} \\ d_i^{(l)} \end{pmatrix} = \underline{N}_i^{(l)} \begin{pmatrix} b_{i-1}^{(l)} \\ d_{i-1}^{(l)} \end{pmatrix} \tag{A3}$$

of the solutions in layer i and the adjacent layer $i-1$ $(i=1,2,3,\ldots,N+1)$ via the boundary matrices

$$\underline{M}_i^{(l)} = \frac{1}{D}\begin{pmatrix} \psi(k_{i-1}r_i)\chi'(k_i r_i) - \frac{n_i}{n_{i-1}}\psi'(k_{i-1}r_i)\chi(k_i r_i) & \chi(k_{i-1}r_i)\chi'(k_i r_i) - \frac{n_i}{n_{i-1}}\chi'(k_{i-1}r_i)\chi(k_i r_i) \\ -\psi(k_{i-1}r_i)\psi'(k_i r_i) + \frac{n_i}{n_{i-1}}\psi'(k_{i-1}r_i)\psi(k_i r_i) & -\chi(k_{i-1}r_i)\psi'(k_i r_i) + \frac{n_i}{n_{i-1}}\chi'(k_{i-1}r_i)\psi(k_i r_i) \end{pmatrix},$$

$$\underline{N}_i^{(l)} = \frac{1}{D}\begin{pmatrix} \frac{n_i}{n_{i-1}}\psi(k_{i-1}r_i)\chi'(k_i r_i) - \psi'(k_{i-1}r_i)\chi(k_i r_i) & \frac{n_i}{n_{i-1}}\chi(k_{i-1}r_i)\chi'(k_i r_i) - \chi'(k_{i-1}r_i)\chi(k_i r_i) \\ -\frac{n_i}{n_{i-1}}\psi(k_{i-1}r_i)\psi'(k_i r_i) + \psi'(k_{i-1}r_i)\psi(k_i r_i) & -\frac{n_i}{n_{i-1}}\chi(k_{i-1}r_i)\psi'(k_i r_i) + \chi'(k_{i-1}r_i)\psi(k_i r_i) \end{pmatrix}. \tag{A4}$$

Here, $D=\psi(k_i r_i)\chi'(k_i r_i)-\psi'(k_i r_i)\chi(k_i r_i)$ is the common denominator and the prime indicates the differentiation. Overall, the amplitudes in the outer medium and the amplitudes in the core are connected by the matrix products $\underline{M}^{(l)} = \underline{M}_{N+1}^{(l)} \cdot \underline{M}_N^{(l)} \cdot \cdots \cdot \underline{M}_1^{(l)}$ and $\underline{N}^{(l)} = \underline{N}_{N+1}^{(l)} \cdot \underline{N}_N^{(l)} \cdot \cdots \cdot \underline{N}_1^{(l)}$. Since $\chi_l(kr)$ becomes infinite at $kr=0$ it cannot be present in the solution in the core and therefore $c_{N+1}^{(l)} = d_{N+1}^{(l)} = 0$. In the surrounding medium, the expansion of an incident unit planar wave as a superposition of spherical waves contributes as

$$rR_{1,\mathrm{in}}^{(l)}(r) = \psi_l(k_0 r)/k_0^2,$$

$$rR_{2,\mathrm{in}}^{(l)}(r) = \psi_l(k_0 r)n_0/k_0^2. \tag{A5}$$

Again the $\chi_l(kr)$ term vanishes since the plane wave remains finite at $kr=0$. The linear combinations $\zeta_l(kr)=\psi_l(kr)+i\chi_l(kr)$ and $\xi_l(kr)=\psi_l(kr)-i\chi_l(kr)$ are identified as outgoing and incoming spherical waves from their asymptotic behavior. Only the outgoing part $\zeta_l(kr)$ is present in the scattered wave with the unknown amplitudes $-a_l$ and $-b_l$ for the two polarization modes:

$$rR_{1,\mathrm{scat}}^{(l)}(r) = -a_l[\psi_l(k_0 r) + i\chi_l(k_0 r)]/k_0^2,$$

$$rR_{2,\mathrm{scat}}^{(l)}(r) = -b_l[\psi_l(k_0 r) + i\chi_l(k_0 r)]n_0/k_0^2. \tag{A6}$$

Combining the contributions in the outer medium via the boundary matrices with the wave in the core yields the two equations

$$\begin{pmatrix} a_{N+1}^{(l)} \\ 0 \end{pmatrix} = \underline{M}^{(l)} \begin{pmatrix} 1 - a_l \\ -ia_l \end{pmatrix} \tag{A7}$$

and

$$\begin{pmatrix} b_{N+1}^{(l)} \\ 0 \end{pmatrix} = \underline{N}^{(l)} \begin{pmatrix} 1 - b_l \\ -ib_l \end{pmatrix}. \tag{A8}$$

Finally, a_l and $a_{N+1}^{(l)}$ are extracted from Eqs. (A7) and (A8) is solved for b_l and $b_{N+1}^{(l)}$. This yields

$$a_l = \frac{M_{21}^{(l)}}{M_{21}^{(l)} + iM_{22}^{(l)}} \tag{A9}$$

and

$$b_l = \frac{N_{21}^{(l)}}{N_{21}^{(l)} + iN_{22}^{(l)}}, \tag{A10}$$

with the matrix elements M_{21}, M_{22}, N_{21}, and N_{22} of the boundary matrices $\underline{M}^{(l)}$ and $\underline{N}^{(l)}$.

A first remark concerns the difference of the eigenmodes of the particles (TE and TM waves for all l) and the eigenmodes of a scattering experiment (s and p polarization). Since s and p polarization couple to the TE modes as well as to the TM modes of the particles, the amplitude coefficients a_l and b_l are present in both, S_1 and S_2 [see Eq. (3)].

The second remark offers a physical picture. A representation where $\psi_l(kr)$ and $\chi_l(kr)$ are replaced by the appropriate combinations of $\zeta_l(kr)$ and $\xi_l(kr)$ in all equations provides a description in analogy to the reflection of plane waves at a planar boundary. Here, for each l there is an incoming spherical wave which is partly transmitted and partly reflected at each layer boundary. The scattered wave is the sum of the reflected outgoing spherical waves for all l.

[1] See, e.g., D. F. Evans and H. Wennerström, *The Colloidal Domain* (Wiley, New York, 1999).

[2] C. Bertozzi and L. L. Kiessling, Science **291**, 2357 (2001).

[3] N. Dingenouts, S. Seelenmeyer, I. Deike, S. Rosenfeldt, M. Ballauff, P. Lindner, and T. Narayanan, Phys. Chem. Chem. Phys. **3**, 1169 (2001).

[4] S. Rosenfeldt, A. Wittemann, M. Ballauff, E. Breininger, J. Bolze, and N. Dingenouts, Phys. Rev. E **70**, 061403 (2004).

[5] S. Seelenmeyer, I. Deike, S. Rosenfeldt, Ch. Norhausen, N. Dingenouts, M. Ballauff, T. Narayanan, and P. Lindner, J. Chem. Phys. **114**, 10471 (2001).

[6] W. Groenewegen, S. U. Egelhaaf, A. Lapp, and J. R. C. van der Maarel, Macromolecules **33**, 3283 (2000).

[7] S. Förster, N. Hermsdorf, C. Böttcher, and P. Lindner, Macromolecules **35**, 4096 (2002).

[8] F. Muller, P. Guenoun, M. Delsanti, B. Deme, L. Auvray, J. Yang, and J. W. Mays, Eur. Phys. J. E **15**, 465 (2004).

[9] K. Gille, H. Knoll, F. Rittig, G. Fleischer, and J. Kärger, Langmuir **15**, 1059 (1999).

[10] H. G. Schild, Prog. Polym. Sci. **17**, 163 (1992).

[11] R. Das, T. T. Mills, L. W. Kwok, G. S. Maskel, I. S. Millett, S. Doniach, K. D. Finkelstein, D. Herschlag, and L. Pollack, Phys. Rev. Lett. **90**, 188103 (2003).

[12] L. Zhang, R. J. Barlow, and A. Eisenberg, Macromolecules **28**, 6055 (1995).

[13] E. G. M. Pelssers, M. A. Cohen Stuart, and G. J. Fleer, J. Colloid Interface Sci. **137**, 350 (1990); H. Lichtenfeld, L. Knapschinsky, C. Dürr, and H. Zastrow, Prog. Colloid Polym. Sci. **104**, 148 (1997).

[14] G. B. Sukhorukov, E. Donath, H. Lichtenfeld, E. Knippel, M. Knippel, A. Budde, and H. Möhwald, Colloids Surf., A **137**, 253 (1998).

[15] R. M. A. Azzam and N. M. Bashara, *Ellipsometry and Polarized Light* (Elsevier Science Publisher, Amsterdam, 1992).

[16] D. E. Aspnes and J. B. Theeten, Phys. Rev. Lett. **43**, 1046 (1979).

[17] Th. A. Germer, Phys. Rev. Lett. **85**, 349 (2000).

[18] M. Kerker, *The Scattering of Light and other Electromagnetic Radiation* (Academic Press, San Diego, 1969).

[19] C. F. Bohren and D. R. Huffman, *Absorption and Scattering of Light by Small Particles* (Wiley, New York, 1998).

[20] An example for the latter case occurs for $\lambda = 633$ nm and vanishing shell thickness.

[21] K. Tauer and V. Khrenov, Macromol. Symp. **179**, 27 (2002).

[22] M. Schönhoff, A. Larsson, P. B. Wetzel, and D. Kuckling, J. Phys. Chem. B **106**, 7800 (2002).

[23] W. H. Press, S. A. Teukolsky, W. T. Vetterling, and B. P. Flannery, *Numerical Recipes in C*, 2nd Ed. (Cambridge University Press, New York, 1992).

[24] *Polymer Handbook*, 4th Ed., edited by J. Brandrup, E. H. Immergut, and E. A. Grulke (Wiley, New York, 1999).

[25] See, e.g., B. J. Berne and R. Pecora, *Dynamic Light Scattering* (Dover Publications, Mineola, NY, 2000).

[26] R. S. Chen, H. Yang, X. H. Yan, Z. L. Wang, and L. Li, Chem. J. Chin. U. **22**, 1262 (2001).

[27] J. Lekner, *Theory of Reflection* (Martinus Nijhoff Publishers, Dordrecht, 1987).